Transportation Research Part D 38 (2015) 156–165

Contents lists available at ScienceDirect

Transportation Research Part D

journal homepage: www.elsevier.com/locate/trd

Ultrafine particle infiltration into passenger vehicles. Part I: Experimental evidence

Eon S. Lee [a,b], Michael K. Stenstrom [b,c], Yifang Zhu [a,c,*]

[a] Department of Environmental Health Sciences, Jonathan and Karin Fielding School of Public Health, University of California Los Angeles, Los Angeles, CA 90095-1772, USA
[b] Department of Civil and Environmental Engineering, Henry Samueli School of Engineering and Applied Science, University of California Los Angeles, Los Angeles, CA 90095-1593, USA
[c] Institute of Environment and Sustainability, University of California Los Angeles, Los Angeles, CA 90095-1772, USA

ARTICLE INFO

Article history:
Available online 23 May 2015

Keywords:
Ultrafine particle
Infiltration
Leakage
In-cabin
Passenger
Automobile

ABSTRACT

Previous studies have reported ultrafine particle (UFP) infiltration to the in-cabin microenvironment; however, no systematic measurements have been conducted showing where and under what conditions infiltration occurs. This study examined the automotive envelope leakage and UFP infiltration. We measured the differential pressures between the cabin and the potential leakage area on the surface of 11 passenger vehicles of different models/-makers. To identify location of infiltration, UFP concentrations were concurrently measured inside and outside the vehicles as well as near the rear trunks. This study found that UFP infiltration primarily occurs through the rear trunk leakage under recirculation (RC) mode. Under RC mode, aerodynamic effects of a moving vehicle made the surface pressure on the side doors lower (i.e., exfiltration) than the cabin pressure, but higher (i.e., infiltration) on the rear trunk. The UFP concentrations measured near the rear trunks were 2–9 folds higher than inside vehicles. The magnitude of pressure differences increased at higher driving speeds. Under outdoor air (OA) mode, the infiltration was rarely observed because of the fan-controlled cabin pressurization. These data provide the first experimental evidence showing that UFP infiltration into passenger vehicles is location-specific and driving-speed-dependent.

© 2015 Elsevier Ltd. All rights reserved.

Introduction

Ultrafine particle (UFP) concentration is usually an order of magnitude higher on roadways than in an urban background (Morawska et al., 2008). Commuters often experience high UFP concentrations in the automotive cabin because of proximity to emissions, high air exchange rate (AER) (Park et al., 1998), leakage of the vehicle envelope (Chan et al., 2002; Esber et al., 2007), and low cabin air filter efficiency (Xu et al., 2011). Recent studies explored exposure mitigation strategies to reduce passenger exposures to UFPs (Lee and Zhu, 2014; Tartakovsky et al., 2013). However, the commuting exposure alone still accounts for 10–50% of the total daily exposure to UFPs (Fruin et al., 2008; Zhu et al., 2007).

AER is an important parameter that accounts for all routes of air exchange and explains overall pollutant transport into the vehicle cabin. Most of previous studies adopted the tracer gas decay method (ASTM, 2011a; Sherman, 1990) and found

* Corresponding author at: Department of Environmental Health Sciences, Jonathan and Karin Fielding School of Public Health, University of California Los Angeles, Los Angeles, CA 90095-1772, USA. Tel.: +1 310 825 4324; fax: +1 310 794 2106.
E-mail address: Yifang@ucla.edu (Y. Zhu).

http://dx.doi.org/10.1016/j.trd.2015.04.025
1361-9209/© 2015 Elsevier Ltd. All rights reserved.

that the in-cabin AER differs by vehicle models, ventilation modes – outdoor air (OA) and recirculation (RC) modes, fan settings, and driving speeds (Hudda et al., 2012; Knibbs et al., 2009; Ott et al., 2008). The RC mode AER is also a function of the manufacturer origin country, vehicle age, mileage, and driving speed (Fruin et al., 2011). Saber and Bazargan (2011) summarized the reported in-cabin AERs in previous studies.

However, AER by itself does not sufficiently explain UFP infiltration into the passenger cabin. First, AER from the tracer gas tests does not take into account particle loss during infiltration processes. In a lab-scale automotive leakage study, Xu et al. (2010) demonstrated that a substantial amount of particle loss occurs (i.e., 5–40%) through idealized automobile cracks. Infiltrated UFP concentrations varied as a function of particle size, leakage geometry, and pressure difference. Particularly in freeway environments, the infiltrated UFP concentrations can be different because a large fraction of UFPs carry electric charges (Lee et al., 2012). Second, AER is not specific to leakage locations; whereas, the infiltration is. A moving vehicle experiences aerodynamic effects, which can affect surface pressures. The surface pressure can increase or decrease as a function of driving speed, but it is also specific to the locations. The surface pressure of a moving vehicle becomes relatively lower on side doors than on the rear trunk (Kang et al., 2012; Song et al., 2012; Tilch et al., 2008). Thus, infiltration can also depend on the leakage location.

In addition to the driving speed, the leakage airflow rate could also change due to cabin pressurization under mechanical ventilation conditions (e.g., OA mode). Therefore, it is important to take into account the ventilation modes, fan settings, driving speed, and vehicle shape when studying automotive envelope leakage and UFP infiltration to the passenger cabin.

From the fluid mechanics perspective, the envelope leakage can be described in a power-law correlation with two parameters: the flow coefficient (C_f) and the pressure exponent (n) (ASHRAE, 2005; ASTM, 2010). These two parameters can be obtained based on the measurements of supplied ventilation airflow rate (Q_{vent}) and the associated changes in differential pressure (dP). This method is commonly applied to study building envelope leakages (Baker et al., 1987; Jeong et al., 2008; Jokisalo et al., 2009) and the same principle applies to automotive envelope leakage (Fletcher and Saunders, 1994). Leakage characterization using this method is also advantageous to determine an equivalent leakage area (ELA) for complex leakage geometry.

In this study, 11 different vehicles were tested to investigate UFP infiltration under both stationary and mobile conditions. This study provides experimental evidences to explain how and under what condition UFP infiltration can occur. In our companion paper (Lee et al., 2015), an in-cabin air quality model was developed to quantitatively examine the effects of UFP infiltration on passenger exposures.

Methodology

Vehicle selections and quartile fan settings

The selected vehicles were different in model, maker, type, size, age, and mileage. Instead of recruiting a representative fleet, this study aimed to characterize the automotive envelope leakage in a broad range of vehicles with different blower fan capacity. The test vehicle models had the total cabin volume size ranging from 2.77 to 7.03 m^3 (U.S.EPA, 2012). These vehicles had age and mileage ranging from 1 to 12 years and 31,000 to 261,000 km, respectively. They also have a wide variety of fan setting scales ranging from a minimum of 1–4 to a maximum of 1–12. To achieve comparable fan settings among tested vehicles, a quartile scale was used. In both OA and RC modes, four evenly distributed fan settings (noted as Q1, Q2, Q3, and Q4) were used with Q1 and Q4 representing the minimum and the maximum, respectively. In addition, no mechanical ventilation condition (i.e. Qoff) was also tested. The test vehicle specifications are tabulated in Table 1.

Instrumentation

The ventilation airflow rate and the differential pressure can characterize the automotive envelope leakage in a power-law correlation. The ventilation airflow rate was measured with a ventilation meter (Q-trak model 7565-X with model 960, TSI Inc., Shoreview, MN) secured on the in-cabin air inlet diffuser. Two manometers (Model HD755, Extech Instruments Co., Nashua, NH) were used to measure the differential pressures between the cabin and the potential leakage area on the vehicle surface: side door gaps and rear trunk gaps, with an accuracy of ±1 Pa. It is noted that the leakage areas in this study were first determined at the gaps on the side doors and rear trunk using stannic chloride ($SnCl_4$) smoke tubes (model 9500, Nextteq LLC., Tampa, FL). The differential pressure measurements were carried out concurrently at the pressure sampling locations: 2 and 4 as well as 1 and 3 (as noted in Fig. 1).

Three sets of condensation particle counters (CPCs) measured UFP number concentrations concurrently at three locations: the center of vehicle cabin ($C_{in\text{-}cabin}$), ambient/on-roadway ($C_{on\text{-}road}$), and inside the cabin but at the rear trunk gap (C_{trunk}). A CPC (Model 3785, TSI Inc., Shoreview, MN) monitored $C_{in\text{-}cabin}$, while another CPC (Model 3786, TSI Inc., Shoreview, MN) monitoring $C_{on\text{-}road}$. The third CPC (Model 3007, TSI Inc., Shoreview, MN) detected the UFP infiltration through the rear trunk leakage (i.e., C_{trunk}). The CPC instruments were collocated before and after field sampling for data quality assurance. Good correlations were observed among the three units (see Supporting Information S1). For the mobile experiments, the driving speed and the coordinates were logged by a GPS unit (Model BT-Q1000XT, QStarz Co. Ltd., Taiwan).

Table 1
A summary of the test vehicle models and specifications: manufacturer (Manuf.), model, year, mileage, vehicle type, cabin volume (U.S.EPA, 2012), quartile fan settings, and leakage parameters (i.e., flow coefficient and pressure exponent). The number in the quartile fan setting represents the tangible fan setting corresponding to the quartile fan setting of the test vehicle model. Q1 is the minimum fan setting, and Q4 is the maximum fan setting; Q4 is equal to the total number of fan settings found in the vehicle models. The numbers in parentheses indicate the ventilation airflow rates (m^3/h) corresponding to each fan setting in OA mode. The asterisks (∗) indicate the five vehicle models used in the mobile measurements.

Manuf.	Model	Year	Mileage (km)	Vehicle type	Cabin volume (m^3)			Quartile fan settings				Leakage parameters	
					Total	Passenger	Cargo	Q1	Q2	Q3	Q4	Flow coefficient (C_f)	Pressure exponent (n)
Ford	Focus	2012	51,000	Hatchback	2.92	2.56	0.36	1 (*110*)	3 (*160*)	5 (*288*)	7 (*335*)	18.78	0.82
Toyota	Corolla*	2005	184,000	Sedan	2.94	2.56	0.39	1 (*58*)	2 (*83*)	3 (*121*)	4 (*176*)	23.39	0.62
	Matrix*	2005	141,000	Hatchback	2.85	2.52	0.33	1 (*73*)	2 (*103*)	3 (*150*)	4 (*221*)	19.71	0.73
	Scion tC*	2008	67,000	Sedan	2.77	2.40	0.37	1 (*84*)	3 (*138*)	5 (*221*)	7 (*298*)	28.70	0.65
	Sienna	2011	68,000	Minivan	5.76	4.66	1.11	1 (*112*)	3 (*229*)	5 (*341*)	6 (*463*)	72.12	0.53
Honda	Civic	2001	261,000	Sedan	2.86	2.49	0.37	1 (*83*)	4 (*157*)	7 (*278*)	9 (*367*)	21.21	0.76
	Accord*	2001	198,000	Sedan	3.28	2.72	0.45	1 (*125*)	5 (*280*)	9 (*452*)	12 (*509*)	23.38	0.85
	Odyssey*	2010	35,000	Minivan	7.03	5.94	1.09	1 (*130*)	3 (*278*)	5 (*440*)	7 (*596*)	31.40	0.75
Mercedes	GL450	2007	58,000	SUV	4.49	4.04	0.45	1 (*80*)	2 (*102*)	4 (*186*)	5 (*315*)	30.71	0.61
BMW	X3	2007	76,000	SUV	3.40	2.55	0.85	1 (*109*)	3 (*169*)	5 (*269*)	8 (*479*)	30.33	0.87
Volkswagen	Cc	2010	31,000	Sedan	3.10	2.73	0.37	1 (*133*)	2 (*202*)	3 (*300*)	4 (*522*)	6.63	1.00

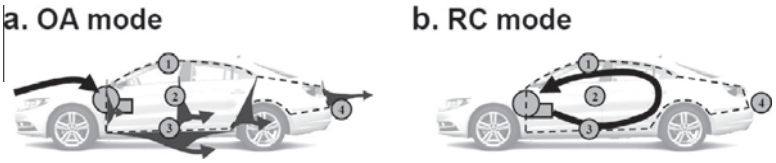

Fig. 1. Graphical illustrations indicate the ventilation airflow path (arrow) in the (a) outdoor air (OA) mode and (b) recirculation (RC) mode. OA-mode ventilation is an open-loop system starting from the outdoor air intake and ending at the exhaust through the side-doors and rear-trunk leakage. RC mode is a close-loop system that utilizes the same cabin air. The total cabin volume is illustrated in dash lines. The circled numbers symbolize the four manometer sensor locations. The differential pressure measurements were named after the number symbols as followed: dP_1, dP_2, dP_3, and dP_4.

Stationary measurements

As opposed to installing a blower-door on a window as used by Fletcher and Saunders (1994), the existing heating/air conditioning blower fan was utilized to pressurize the cabin. The blower fan provided needed cabin pressurization under the OA mode. This approach helps exclude the ventilation system as a potential leakage area. Although the penetration of air pollutants could occur through the ventilation systems, it is usually intended and controlled by choosing the ventilation settings. Thus, the air penetration through ventilation system is not considered as leakage or infiltration in this study; instead, it was regarded as passive ventilation (Ott et al., 2008). In our companion paper (Lee et al., 2015), the effects of passive ventilation on passenger exposures are discussed.

Under stationary condition, the mechanical ventilation flow was only allowed through an open diffuser while the other diffusers were completely sealed with heavy duct tapes. As stepping up the fan settings (and stepping down to verify), the inlet airflow rates were estimated from the measurements of the diffuser area and the average airflow velocity at the center and corners of the diffuser. There is less than 1% of difference of measured airflow velocity between the center and the corners. At the same time, the associated pressure differences between the in-cabin and the ambient were measured. With respect to the ambient pressure, the cabin pressure was uniform at various locations inside the passenger cabin. The measurements were repeated for all test vehicles under 10 possible combinations of the ventilation modes (i.e., OA and RC) and the quartile fan settings (i.e., Q1, Q2, Q3, and Q4) as well as Qoff. All windows were closed during the measurements.

Mobile measurements

To elucidate the aerodynamic effects on in-cabin to surface pressure differences, the ventilation airflow rates were monitored under driving conditions while the GPS tracked driving speed, direction, coordinate, and elevation. The differential pressure measurements were conducted on both freeways and local roadways. The differential pressure changes on the vehicle envelope were monitored at four locations: three around the side door and one on the lateral center of the rear trunk gap (see Fig. 1 for the sampling locations). Each manometer measured the differential pressure (dP_i) in this study, as follows:

$$dP_i = P_{in\text{-}cabin} - P_i \tag{1}$$

where dP_i is the differential pressure between the in-cabin and the sampling location i (Pa), $P_{in\text{-}cabin}$ is the pressure at the center of the passenger cabin (Pa), P_i is the pressure at the sampling location i (Pa), and i is the pressure sampling location at the door/trunk gaps as indicated in Fig. 1 (i.e., i = 1, 2, 3, and 4). In Eq. (1), a positive differential pressure ($dP_i > 0$) indicates cabin pressurization (i.e., $P_{in\text{-}cabin} > P_i$), which leads to exfiltration. Conversely, a negative value ($dP_i < 0$) represents infiltration. The dP_i was found near zero for any given i under the stationary RC condition (see Fig. 2d). When a vehicle driven in RC mode, a positive dP_i is expected due to the aerodynamic effects making P_i lower than $P_{in\text{-}cabin}$. Under the same condition, negative differential pressure ($dP_i < 0$) may occur when $P_i > P_{in\text{-}cabin}$.

The on-road experiments were conducted under four ventilation settings: OA-Qoff, OA-Q4, RC-Qoff, and RC-Q4. These ventilation settings were selected to examine whether infiltration occurs under OA mode when the passenger cabin is

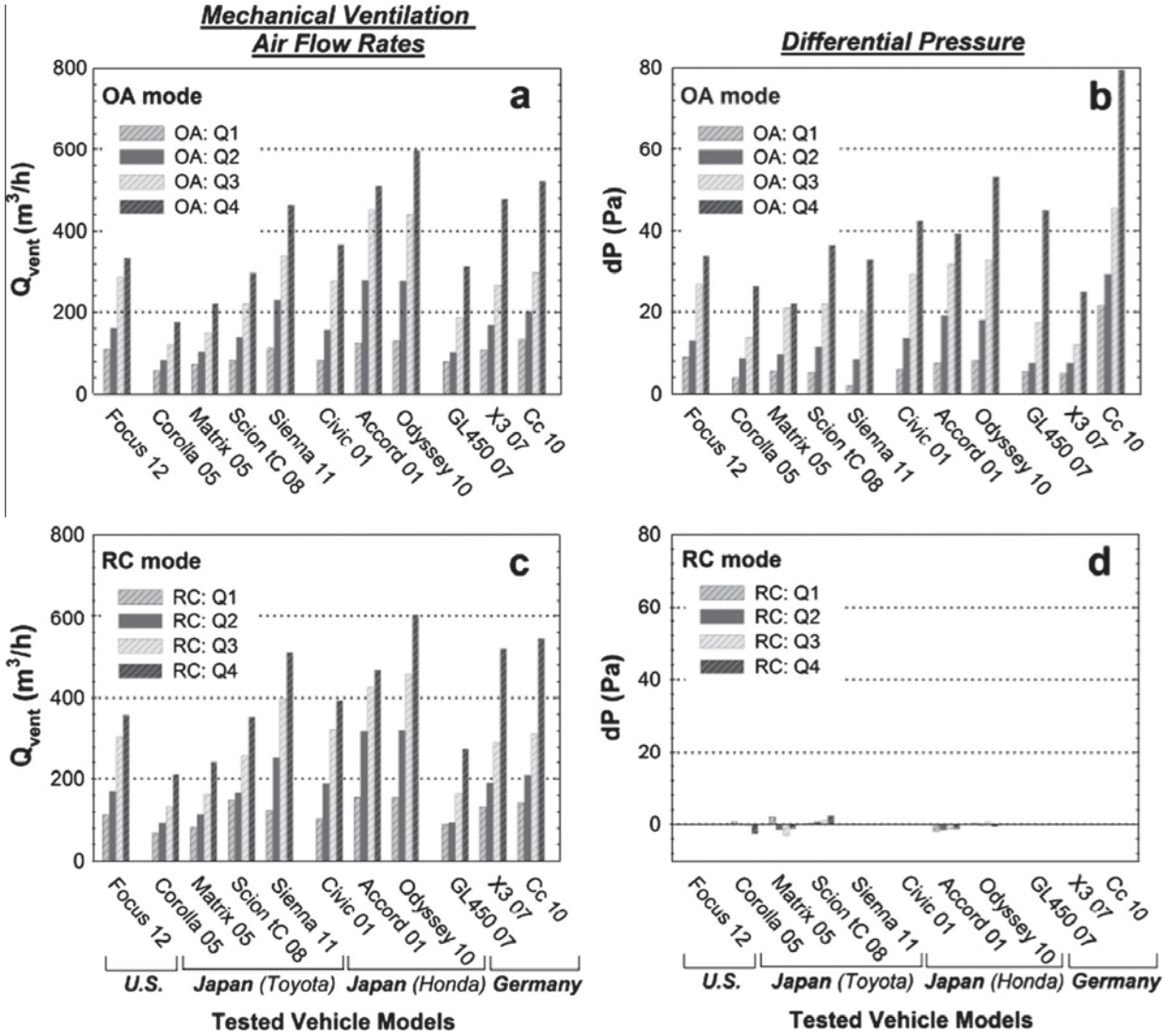

Fig. 2. The mechanical ventilation airflow rates (Q_{vent}, panels a, c) and the associated differential pressures (dP, panels b, d) in the stationary condition are plotted for the OA (on the top) and RC (on the bottom) modes. The different shades indicate the different fan settings (i.e., Q1 through Q4). The x-axis shows the 11 test vehicle models ordered according to the manufacturers (i.e., Ford, Toyota, Honda, Mercedes-Benz, BMW, and Volkswagen) and the origin countries: U.S., Japan, and Germany.

positively pressurized by passive ventilation (i.e., OA-Qoff) and mechanical ventilation (i.e., OA-Q4). Under RC mode, this study examined the same question under neutral cabin pressure with (i.e., RC-Q4) and without (i.e., RC-Qoff) repeated filtration. These measurements were repeated three times on the same driving route for two vehicle types (i.e., sedan and minivan) and four ventilation settings noted above. All measurement data were collected with a 1-s sampling interval for all instruments to capture rapid responses of in-cabin and on-road UFP concentrations (i.e., $C_{in\text{-}cabin}$, C_{trunk}, and $C_{on\text{-}road}$) due to dynamic driving conditions.

Analytical

To characterize automotive envelope leakage, this study adopted the concept of a power-law leakage functions (i.e., power-law correlation) from building environment studies (ASHRAE, 2005; ASTM, 2010; Baker et al., 1987), as shown in Eq. (2).

$$Q_{vent} = C_f \cdot dP^n \tag{2}$$

where Q_{vent} is the ventilation airflow rate (m^3/h), C_f is the flow coefficient ($m^3/s\ Pa^n$), dP is the differential pressure (Pa), and n is the pressure exponent. Based on the measurements of Q_{vent} and dP at a wide range of fan settings under stationary OA mode, two-parameter power-law regression analyses provided semi-empirical estimates of a flow coefficient (C_f) and a pressure exponent (n) for each vehicle model.

Given the values of C_f and n, the equivalent leakage area (ELA) (ASHRAE, 2005; ASTM, 2011b) was estimated at a dP_{ref} of either 20 or 50 Pa. The 20 Pa was used because it was commonly achieved in all 11 vehicle models regardless of blower fan capacities (discussed later in Section "Variability in the mechanical ventilation systems"). The 50 Pa was also used for comparison since it is the commonly used reference pressure in building environment (ASHRAE, 2005). It is important to note that the ELA is not equal to the actual leakage area and it changes slightly as a function of the reference pressure. However, the use of ELA provides a reasonable comparison of the envelope leakage area among different vehicle models at the same reference pressure. Eq. (3) describes the ELA calculation:

$$\text{ELA} = 3.6 \times 10^7 \cdot \frac{C_f}{C_d} \cdot \left(\frac{\rho_{air}}{2}\right)^{1/2} \cdot dP_{ref}^{n-1/2} \tag{3}$$

where ELA is the equivalent leakage area (ELA, cm^2) at a reference pressure, C_f is the flow coefficient ($m^3/s\ Pa^n$) the same as C_f in Eq. (2), C_d is the discharge coefficient (=1.0 $kg^{1/2}/m^{1/2}$ h Pa) (ASHRAE, 2005; ASTM, 2011b), ρ_{air} is the density of air (kg/m^3), and dP_{ref} is the reference differential pressure (Pa).

Results and discussion

Variability in the mechanical ventilation systems

Fig. 2 presents the mechanical ventilation flow rates and the associated differential pressures for the 11 test vehicle models under stationary OA and RC conditions. The maximum mechanical ventilation flow rates (i.e., Q4) ranged from 200 to 600 m^3/h (Fig. 2a and c), indicating that the blower fan capacities are highly variable across different vehicle models. The ventilation mode (i.e., OA or RC) created distinctive differences in both ventilation airflow rate and differential pressure. Overall, the mechanical ventilation flow rates were 13% higher on average (±13% depending on vehicle models) under the RC mode (Fig. 2c) than under the OA mode (Fig. 2a). This is likely because the RC mode airflow cycle does not experience the additional pressure drop at the OA intake manifold.

Fig. 2b shows the cabin pressurization under OA mode. The cabin pressurization reached up to 80 Pa during stationary mode measurements. Although it is clear that the differential pressure is a function of the ventilation inlet airflow rates, its variability across the different vehicle models was high (i.e., 20–80 Pa) under the same quartile fan settings. However, under the RC mode (i.e., closed air damper) of any fan setting, the differential pressure remained near zero (Fig. 2d) within ±3 Pa across the tested vehicle models. This indicates nearly 100% recirculation of the same cabin air; otherwise, the RC mode would have resulted in a certain level of cabin pressurization despite the fan settings or the test vehicle models.

The measured differential pressure of ±3 Pa under the RC mode stationary condition (Fig. 2d) also represents the effects of wind on infiltration. Since mechanical ventilation system does not pressurize the vehicle cabin under the RC mode, the measured differential pressure occurred due to the changes of wind speed and direction. However, the effect of ambient wind is devised to be little under OA mode because OA mode ventilation mechanically increases the cabin pressure up to 80 Pa (Fig. 2b) under the same stationary condition. When a vehicle is moving, the meteorological effects are reduced further because aerodynamic changes induced by driving can increase the differential pressure up to 200 Pa (see Section "Aerodynamic differential pressure changes on moving vehicles" for details).

Leakage function and equivalent leakage area

Fig. 3 presents the power-law leakage functions characterized by the two parameters: the flow coefficient (C_f) and the pressure exponent (n). The power-law correlation between airflow rate and pressure difference has its fundamental basis

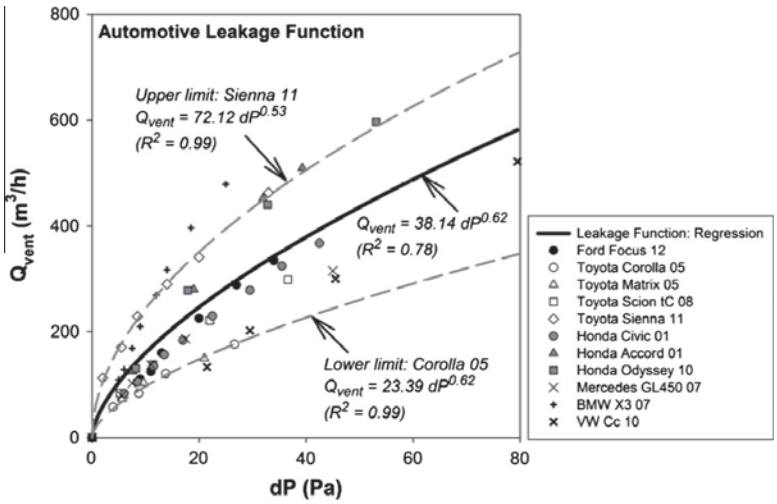

Fig. 3. The stationary measurements of ventilation inlet airflow rate (Q_{vent}) as a function of differential pressure (dP). The dP data were measured at sampling location 3 (i.e., i = 3 in Fig. 1). Note, dP did not change at different sampling locations (i = 1 through 4) under stationary conditions. The different symbols represent the observations from the 11 test vehicle models, and the color schemes indicate the different origin countries and manufacturers: U.S. (black), Japan Toyota (white), and Japan Honda (gray). The German vehicle models are marked with line symbols (e.g., cross). Regression result of the measurements is given in solid line and the upper/lower limits are presented in dash lines.

in the Bernoulli's equation. In case of an orifice flow, n is equal to 0.5 and C_f becomes a function of fluid density (ρ) and cross-sectional area (A) of the flow (i.e., $C_f = A \cdot (2/\rho)^{0.5}$). However, when this concept is applied to building envelope leakage, the value of n can vary from 0.55 to 0.75 because of the complexity of leakage geometry and a value of 0.65 is typically assumed for building cracks (ASHRAE, 2005). In this study, a power-law regression of all 11 test vehicle models yielded C_f and n values of 38.14 and 0.62, respectively. Since the leakage geometry determines the leakage functions, different vehicle models presented a range of leakage function parameters, ranging from 6.63 to 72.12 for C_f and from 0.53 to 1.00 for n. The C_f and n values were determined from stationary measurements and tabulated for the 11 test vehicles in Table 1.

From the power-law correlation, the AER under the OA mode can be calculated from the differential pressure (dP) as shown in Eq. (4). This method assumes well-mixed cabin air because of small cabin volume (V_{cabin}) size and high ventilation airflow rate (Q_{vent}). Previous studies also validated this assumption experimentally (Joodatnia et al., 2013; Ott et al., 2008). The OA AER calculation involves inlet airflow rate (i.e., Q_{vent} in Eq. (2)), which can be estimated at any given dP with the vehicle-specific leakage function parameters (i.e., C_f and n) in Fig. 3 and Table 1. Thus, the OA AER can be calculated in the following form:

$$\text{OA AER} = \frac{Q_{vent}}{V_{cabin}} = \frac{C_f \cdot dP^n}{V_{cabin}} \tag{4}$$

where OA AER is the OA-mode air exchange rate (h^{-1}) and V_{cabin} is the cabin volume (m^3). It should be noted that the dP in Eq. (4) is the differential pressure caused by the mechanically supplied airflow rate (i.e., Q_{vent}); thus, it is independent from the reference pressure difference (dP_{ref}) in Eq. (3).

With the OA AER, this study compared the increase of the OA AER with respect to the envelope leakage area (i.e., ELA) for different vehicle types (i.e., hatchback, sedan, SUV, and minivan) of various vehicle models from different manufacturers. The ELA was estimated at dP_{ref} of 20 Pa using Eq. (3). Different levels of cabin pressurization (i.e., dP = 20 Pa and 50 Pa) provided different Q_{vent} and demonstrated the changes in OA AER with respect to ELA in Fig. 4. Since vehicle models have highly variable fan settings and blower capacity as seen in Fig. 2, it is difficult to achieve the same level of dP for all test vehicle models by controlling the fan settings. Instead, this study used two constant dP values in Eq. (4) (i.e., dP = 20 or 50 Pa) in order to compare the OA AER and ELA across different vehicle models. It shows that the OA AER linearly increases when leakage area (i.e., ELA) becomes larger. Note that higher inlet airflow rate (Q_{vent}) is required to achieve the same level of cabin pressurization for a leakier vehicle. However, higher cabin pressure in Fig. 4 does not always mean proportionally higher OA AER and that was taken into account in Q_{vent} by applying vehicle-specific C_f and n in Eq. (4).

In addition, the rate of OA AER change was specific to the vehicle type because SUV and minivan have larger V_{cabin} than hatchback and sedan. Assuming negligible temperature change during air penetration (Fletcher and Saunders, 1994), the following relationship can be determined based on mass conservation (i.e., $Q_{in} = Q_{out}$):

$$\text{OA AER} = \frac{v_{leakage}}{V_{cabin}} \cdot \text{ELA} \tag{5}$$

where $v_{leakage}$ is the mean leakage airflow velocity (m/h).

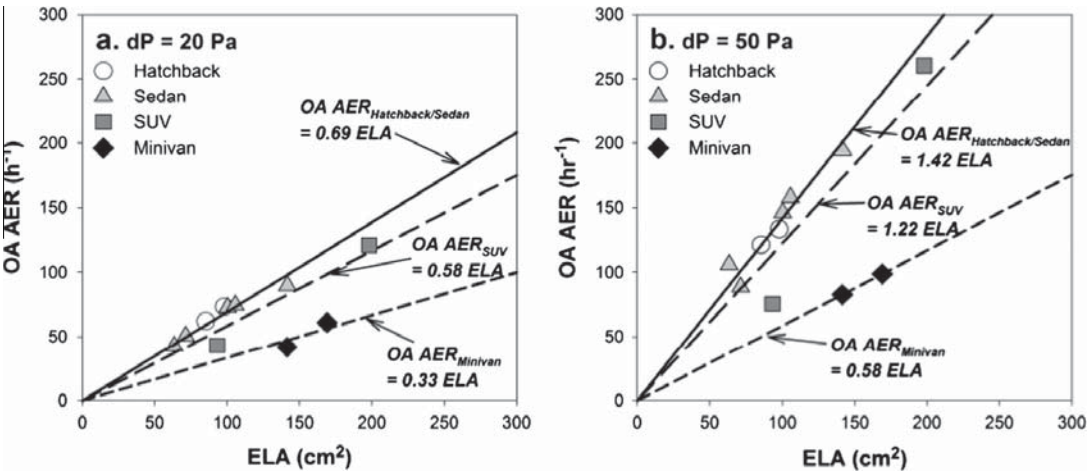

Fig. 4. For the different levels of cabin pressurization (dP) of (a) 20 Pa and (b) 50 Pa, the OA-mode air exchange rates (OA AERs) are compared to the equivalent leakage areas (ELAs) at 20 Pa. The linear relationship between the OA AER and the ELA is presented for hatchback/sedan (solid line), SUV (medium-dash line), and minivan (short-dash line).

Eq. (5) quantitatively verifies the linear correlation observed in Fig. 4. In Fig. 4a, the slope of the linear regression (i.e., $=v_{leakage}/V_{cabin}$) decreased from 0.69 to 0.33 primarily because the V_{cabin} is larger for minivan than hatchback or sedan and the regression line for SUV lies in between the two ($v_{leakage}/V_{cabin} = 0.58$). In Fig. 4b, the increased cabin pressure resulted higher $v_{leakage}/V_{cabin}$ for all vehicle types. For the same vehicle type, greater cabin pressurization at 50 Pa consequently resulted in an overall higher OA AER because of the increased $v_{leakage}$ as shown in Fig. 4a. Therefore, the OA AER is linearly proportional to the ELA and is affected by vehicle types, more specifically V_{cabin}.

Aerodynamic differential pressure changes on moving vehicles

The pressure field on the surface of a moving vehicle (P_i) changes considerably because of the aerodynamic changes at different driving speeds and vehicle shapes. Accordingly, the differential pressure (dP_i) between the cabin and the leakage on the vehicle envelope changes not only by the driving speed but also by the leakage location and vehicle shape. Fig. 5 presents differential pressure data collected under RC mode at a wide range of driving speed. The data were collected in five vehicle models as noted in Table 1. Fig. 5 shows typical measurements for a sedan (2008 Toyota Scion tC, Fig. 5a) and a minivan (2010 Honda Odyssey, Fig. 5b). Under RC mode, air dampers are closed to prevent cabin pressurization from passive

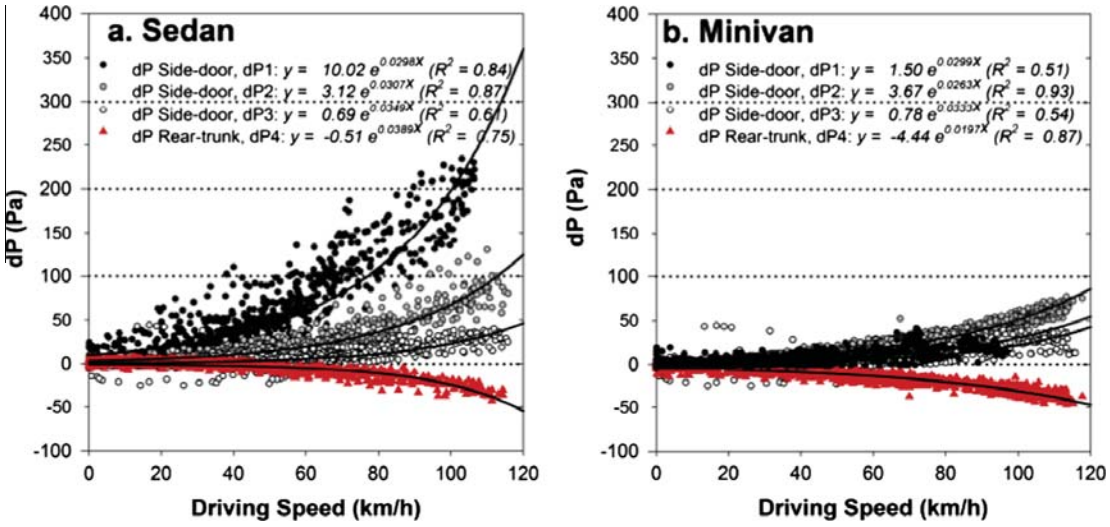

Fig. 5. The differential pressure data at four different leakage locations (see Fig. 1), three on the side door (i.e., dP_1, dP_2, and dP_3) and one on the rear trunk (i.e., dP_4), are plotted as a function of the driving speed. The data are presented with 1-s data for two distinctive vehicle types: (a) sedan (2008 Scion tC) and (b) minivan (2010 Honda Odyssey). The different schemes of symbols and colors indicate the differential pressure monitored at the four locations, and the regression data (lines) are also provided for each dataset. (For interpretation of the references to color in this figure legend, the reader is referred to the web version of this article.)

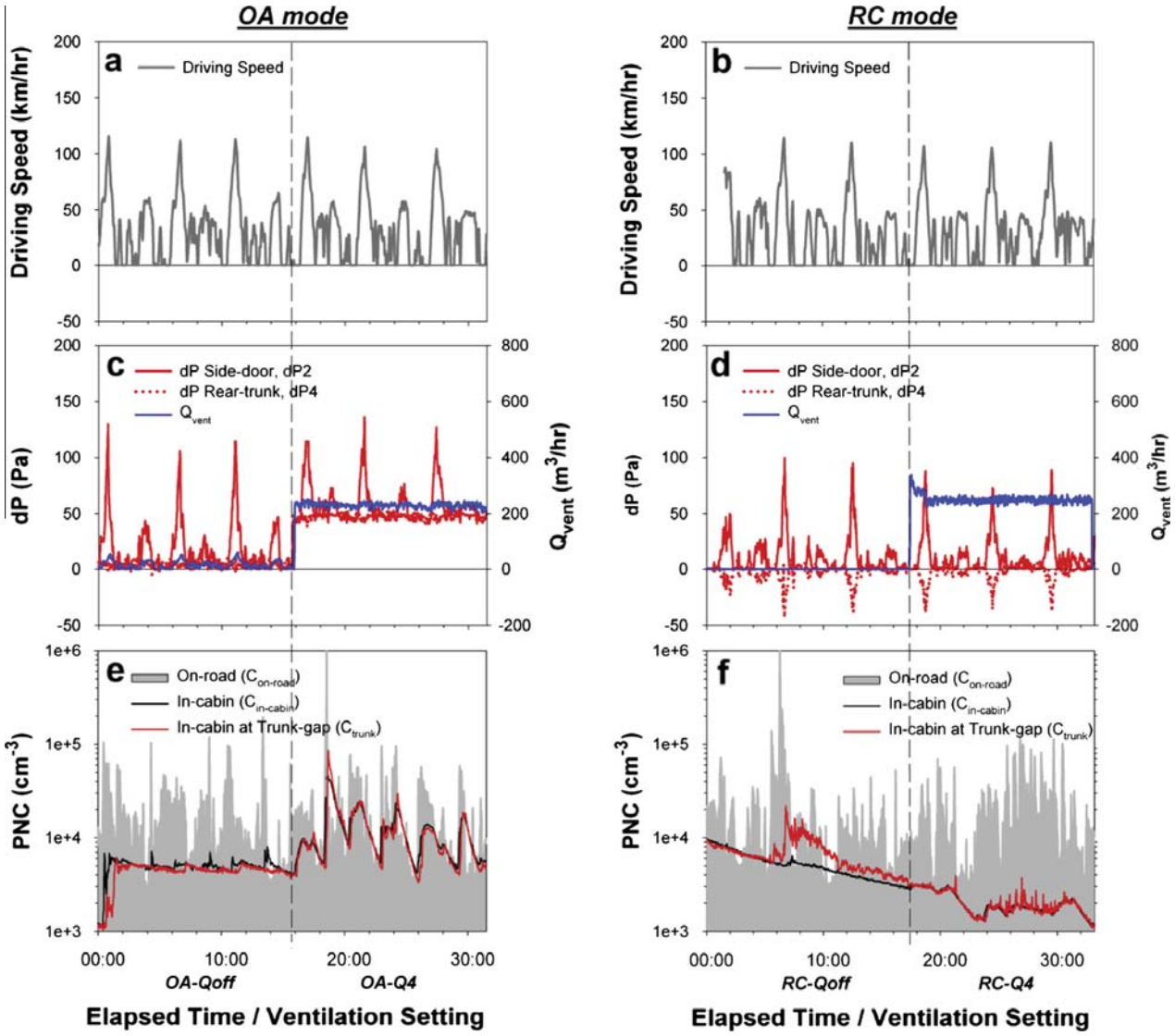

Fig. 6. The driving speed (panels a, d) and the differential pressure and ventilation airflow rates (panels b, e) are plotted in time and compared between OA mode (on the left) and RC mode (on the right). The bottom two panels (panels c, f) provide the corresponding particle number concentrations in on-road ($C_{on\text{-}road}$, gray area) and in-cabin ($C_{in\text{-}cabin}$, black) conditions and compared to the concentration at the rear trunk leakage (C_{trunk}, red). All parameters are presented with 1-s data. (For interpretation of the references to color in this figure legend, the reader is referred to the web version of this article.)

ventilation. Therefore, the data in Fig. 5 are not affected by the cabin pressure but only by the surface pressure changes on the vehicle envelope (i.e., P_i in Eq. (1)).

In terms of UFP infiltration, the leakage at the side doors might not be of great concern, but the leakage at the rear trunk is important. When a vehicle is driven at a high speed, the moving vehicle experiences relatively lower pressure on the side door than in the cabin (i.e., $P_{in\text{-}cabin} > P_i$). In return, the pressure differences (dP_1, dP_2, and dP_3 in Fig. 5) become positive. At the side doors, the low surface pressure field at high speed prevents UFP infiltration through the leakage. In contrast, relatively higher pressure at the surface of rear trunk gap creates a negative differential pressure shown as dP_4 (i.e., $P_{in\text{-}cabin} < P_4$) in both vehicle types. Therefore, UFP infiltration can occur through the leakage route at rear trunk.

The infiltration could be more significant at higher driving speeds because of the exponential increase in the negative differential pressure (i.e., dP_4). The two distinctive vehicle shapes (i.e., sedan and mini-van) had similar results in terms of the magnitude of increase in the differential pressure at the rear trunk (i.e., dP_4 up to -50 Pa at 110 km/h) as a function of the driving speed. When a vehicle is at high speed, the infiltration airflow rate through the leakage of the rear trunk is expected to increase and consequently the passenger cabin environment can become more vulnerable to on-road UFPs. The following section presents more experimental evidence of UFP infiltration based on concurrent measurements of in-cabin and on-road UFP number concentrations.

UFP infiltration in moving vehicles

Fig. 6 provides test results under the OA and RC modes of a moving vehicle (Toyota Scion tC 2008). Supporting Information S2 provides similar results for a minivan (Honda Odyssey 2010). Fig. 6a and b illustrates the driving speed in time-series during each test. The speed ranges from 0 to 120 km/h. In each ventilation mode/fan setting condition (i.e., OA-Qoff, OA-Q4, RC-Qoff, and RC-Q4), the three highest peaks of the driving speed represent the maximum driving speed achieved on the freeway during the three repeated trips. The remaining peaks with a lower magnitude refer to the driving speed on local streets.

Under both OA and RC mode, the fan was set to either Qoff or Q4 to simulate two distinctive fan conditions. Fig. 6c and d provides the comparisons of ventilation flow rates (Q_{vent}) under OA and RC modes, respectively. Under the OA mode, the mechanical ventilation dominated Q_{vent} but the passive ventilation could increase the Q_{vent} at high speed. While the fan is off (i.e., OA-Qoff in Fig. 6c), the oscillation of Q_{vent} tracks changes of speed and differential pressure. This observation was also found at the maximum fan setting (i.e., OA-Q4 in Fig. 6c).

Under the OA mode, passive and mechanical ventilation prevents the infiltration by compensating the negative differential pressure observed at the rear trunk leakage (dP_4) and making the dP_4 positive (Fig. 6c). The cabin pressurization under OA mode substantially maintained positive dP_4; however negative dP_4 was commonly observed under RC mode (Fig. 6d) at the rear trunk leakage. Even without fan-operation, the passive ventilation alone reduced the differential pressure by 50 Pa in OA-Qoff. The introduction of mechanical ventilation in the OA-Q4 mode (Fig. 6c) further increased the differential pressures on both the side doors and the rear trunk. Consequently, Fig. 6e provided nearly identical particle number concentrations in the in-cabin ($C_{in\text{-}cabin}$) and at the rear trunk leakage (C_{trunk}). It suggests that the in-cabin air exhausted through the rear-trunk leakage due to the positive cabin pressure under the OA mode.

Under the RC mode, however, the negative differential pressure at the rear trunk leakage (dP_4) is present at all time and consequently triggers the UFP infiltration. Once again, cabin air recirculation in this ventilation mode maintains in and out pressure different near zero when vehicles are in stationary condition (as shown in Fig. 2d). The observation of negative differential pressure in Fig. 6d occurred from the aerodynamic changes (e.g., driving speed). Corresponding to the negative pressure under the RC mode, the infiltrated UFP concentration was much higher at the rear trunk leakage than at the center of passenger cabin. Fig. 6f shows that C_{trunk} was greater than $C_{in\text{-}cabin}$. The peaks of the C_{trunk} in the RC-Qoff mode clearly demonstrate that the C_{trunk} are 2–4 folds higher than $C_{in\text{-}cabin}$. Supporting Information S2 shows similar findings from a minivan. In that case, C_{trunk} was up to 9-fold higher than $C_{in\text{-}cabin}$. From the observations in both differential pressure and particle number concentration at the leakage, it is concluded that the UFP infiltration physically occurs at high speed under RC mode ventilation conditions.

Conclusions

This paper presented the data collected from 11 vehicle models on automotive envelope leakage and UFP infiltration to passenger cabins. The automotive envelope leakage functions were characterized with the flow coefficient (C_f) and the pressure exponent (n). Using the automotive leakage function, this study quantitatively and experimentally demonstrated that the OA mode AER is linearly proportional to the ELA. The UFP infiltration depends on the combined effects of the ventilation conditions (i.e., ventilation mode and fan settings) and the aerodynamic changes on the vehicle envelope (i.e., driving speed and vehicle shapes). Pressure measurement data showed that UFP infiltration can physically occur through the rear trunk leakage route but is less likely to occur through side doors. UFP concentration measurements demonstrated that the infiltrated UFP concentrations were about 9-fold higher than in-cabin concentration under RC mode. Even with the high blower fan setting used in the RC-Q4 mode (i.e., highly repeated filtration), the infiltrated UFPs were still observed at the rear trunk leakage.

UFP infiltration is a dynamic process, which depends on the surface pressure at the rear trunk leakage, in-cabin pressure, and the ambient concentration on the roadway. Properly maintained cabin pressurization in OA mode may prevent UFP to infiltrate into the passenger cabin through vehicle cracks. However, one should note that OA-mode cabin pressurization does not necessarily mean lower in-cabin UFP concentrations because UFPs are present in the mechanical ventilation air even after filtration. For more quantitative analysis, a companion paper presented a mathematical model to evaluate the effects of different pollutant transport mechanisms, including UFP infiltration, on passenger exposures and discussed its dependency on ventilation condition and driving speed (Lee et al., 2015).

Acknowledgments

This study complements work in progress supported by the National Science Foundation's CAREER Award under contract # 32525-A6010 AI. The authors thank two automobile engineers from Toyota and Hyundai for providing technical advice on automotive ventilation systems. Any opinions, findings, conclusions or recommendations expressed in this report are those of the authors and do not necessarily reflect the views of the National Science Foundation.

Appendix A. Supplementary material

Supplementary data associated with this article can be found, in the online version, at http://dx.doi.org/10.1016/j.trd.2015.04.025.

References

ASHRAE, 2005. ASHRAE Handbook: 2005 Fundamentals. American Society of Heating, Refrigerating, and Air-Conditioning Engineers, Atlanta, GA.

ASTM, 2010. E779-10 Standard Test Method for Determining Air Leakage Rate by Fan Pressurization. ASTM International, West Conshohocken, PA.

ASTM, 2011a. E741-11 Standard Test Method for Determining Air Change in a Single Zone by Means of a Tracer Gas Dilution. ASTM International, West Conshohocken, PA.

ASTM, 2011b. E1827-11 Standard Test Methods for Determining Airtightness of Buildings Using an Orifice Blower Door. ASTM International, West Conshohocken, PA.

Baker, P.H., Sharples, S., Ward, I.C., 1987. Air-flow through cracks. Build. Environ. 22 (4), 293–304.

Chan, L.Y., Lau, W.L., Zou, S.C., Cao, Z.X., Lai, S.C., 2002. Exposure level of carbon monoxide and respirable suspended particulate in public transportation modes while commuting in urban, area of Guangzhou, China. Atmos. Environ. 36 (38), 5831–5840.

Esber, L.A., El-Fadel, M., Nuwayhid, I., Saliba, N., 2007. The effect of different ventilation modes on in-vehicle carbon monoxide exposure. Atmos. Environ. 41 (17), 3644–3657.

Fletcher, B., Saunders, C.J., 1994. Air change rates in stationary and moving motor-vehicles. J. Hazard. Mater. 38 (2), 243–256.

Fruin, S., Westerdahl, D., Sax, T., Sioutas, C., Fine, P.M., 2008. Measurements and predictors of on-road ultrafine particle concentrations and associated pollutants in Los Angeles. Atmos. Environ. 42 (2), 207–219.

Fruin, S.A., Hudda, N., Sioutas, C., Defino, R.J., 2011. Predictive model for vehicle air exchange rates based on a large, representative sample. Environ. Sci. Technol. 45 (8), 3569–3575.

Hudda, N., Eckel, S.R., Knibbs, L.D., Sioutas, C., Delfino, R.J., Fruin, S.A., 2012. Linking in-vehicle ultrafine particle exposures to on-road concentrations. Atmos. Environ. 59, 578–586.

Jeong, J.W., Firrantello, J., Bahnfleth, W.P., Freihaut, J.D., Musser, A., 2008. Case studies of building envelope leakage measurement using an air-handier fan pressurisation approach. Build. Serv. Eng. Res. Technol. 29 (2), 137–155.

Jokisalo, J., Kurnitski, J., Korpi, M., Kalamees, T., Vinha, J., 2009. Building leakage, infiltration, and energy performance analyses for Finnish detached houses. Build. Environ. 44 (2), 377–387.

Joodatnia, P., Kumar, P., Robins, A., 2013. Fast response sequential measurements and modelling of nanoparticles inside and outside a car cabin. Atmos. Environ. 71, 364–375.

Kang, S.O., Jun, S.O., Park, H.I., Song, K.S., Kee, J.D., Kim, K.H., Lee, D.H., 2012. Actively translating a rear diffuser device for the aerodynamic drag reduction of a passenger car. Int. J. Automot. Technol. 13 (4), 583–592.

Knibbs, L.D., de Dear, R.J., Atkinson, S.E., 2009. Field study of air change and flow rate in six automobiles. Indoor Air 19 (4), 303–313.

Lee, E.S., Zhu, Y.F., 2014. Application of a high-efficiency cabin air filter for simultaneous mitigation of ultrafine particle and carbon dioxide exposures inside passenger vehicles. Environ. Sci. Technol. 48 (4), 2328–2335.

Lee, E.S., Xu, B., Zhu, Y.F., 2012. Measurements of ultrafine particles carrying different number of charges in on- and near-freeway environments. Atmos. Environ. 60, 564–572.

Lee, E.S., Stenstrom, M.K., Zhu, Y.F., 2015. Ultrafine particle infiltration into passenger vehicles. Part II: model analysis. Transp. Res. Part D: Transp. Environ. 38, 144–155.

Morawska, L., Ristovski, Z., Jayaratne, E.R., Keogh, D.U., Ling, X., 2008. Ambient nano and ultrafine particles from motor vehicle emissions: characteristics, ambient processing and implications on human exposure. Atmos. Environ. 42 (35), 8113–8138.

Ott, W., Klepeis, N., Switzer, P., 2008. Air change rates of motor vehicles and in-vehicle pollutant concentrations from secondhand smoke. J. Expos. Sci. Environ. Epidemiol. 18 (3), 312–325.

Park, J.H., Spengler, J.D., Yoon, D.W., Dumyahn, T., Lee, K., Ozkaynak, H., 1998. Measurement of air exchange rate of stationary vehicles and estimation of in-vehicle exposure. J. Expos. Anal. Environ. Epidemiol. 8 (1), 65–78.

Saber, E.M., Bazargan, M., 2011. Dynamic behavior modeling of cigarette smoke particles inside the car cabin with different ventilation scenarios. Int. J. Environ. Sci. Technol. 8 (4), 747–764.

Sherman, M.H., 1990. Tracer-gas techniques for measuring ventilation in a single zone. Build. Environ. 25 (4), 365–374.

Song, K.S., Kang, S.O., Jun, S.O., Park, H.I., Kee, J.D., Kim, K.H., Lee, D.H., 2012. Aerodynamic design optimization of rear body shapes of a sedan for drag reduction. Int. J. Automot. Technol. 13 (6), 905–914.

Tartakovsky, L., Baibikov, V., Czerwinski, J., Gutman, M., Kasper, M., Popescu, D., Veinblat, M., Zvirin, Y., 2013. In-vehicle particle air pollution and its mitigation. Atmos. Environ. 64, 320–328.

Tilch, R., Tabbal, A., Zhu, M., Decker, F., Lohner, R., 2008. Combination of body-fitted and embedded grids for external vehicle aerodynamics. Eng. Comput. 25 (1–2), 28–41.

U.S.EPA, 2012. Fuel Economy Database. U.S. EPA.

Xu, B., Liu, S., Zhu, Y., 2010. Ultrafine particle penetration through idealized vehicle cracks. J. Aerosol Sci. 41 (9), 859–868.

Xu, B., Liu, S.S., Liu, J.J., Zhu, Y.F., 2011. Effects of vehicle cabin filter efficiency on ultrafine particle concentration ratios measured in-cabin and on-roadway. Aerosol Sci. Technol. 45 (2), 234–243.

Zhu, Y.F., Eiguren-Fernandez, A., Hinds, W.C., Miguel, A.H., 2007. In-cabin commuter exposure to ultrafine particles on Los Angeles freeways. Environ. Sci. Technol. 41 (7), 2138–2145.